COMPRESSIVE CHARACTERISATION OF SINGLE CARBON FIBRES AND THEIR COMPOSITE INTERFACES VIA *IN SITU* RAMAN SPECTROSCOPY

Cameron.G. Woodgate[1], Richard.S. Trask[2], Milo.S.P. Shaffer[3] and Stephen.J. Eichhorn[4]

[1] Bristol Composites Institute, School of Civil, Aerospace and Mechanical Engineering, University of Bristol, University Walk, Bristol, BS8 1TR, UK, cameron.woodgate@bristol.ac.uk

[2] Bristol Composites Institute, School of Civil, Aerospace and Mechanical Engineering, University of Bristol, University Walk, Bristol, BS8 1TR, UK, r.s.trask@bristol.ac.uk, https://research-information.bris.ac.uk/en/persons/richard-s-trask

[3] Department of Materials and Department of Chemistry, Imperial College London, South Kensington Campus, London, SW7 2AZ, UK, m.shaffer@imperial.ac.uk, https://www.imperial.ac.uk/people/m.shaffer

[4] Bristol Composites Institute, School of Civil, Aerospace and Mechanical Engineering, University of Bristol, University Walk, Bristol, BS8 1TR, UK, s.j.eichhorn@bristol.ac.uk, https://research-information.bris.ac.uk/en/persons/steve-eichhorn

Keywords*:* Raman spectroscopy, Compression, Carbon fibre, Micromechanics, Interfacial analysis

ABSTRACT

A current design limiting aspect of unidirectional carbon fibre reinforced polymer composites is their lack of strength in compression compared to tensile loading. To improve the compressive performance of carbon fibre reinforced polymer, it is critical to understand how failure occurs at each constituent length scale. One way to achieve this is to produce model composites, which address this at the single fibre level.

In this study, Raman spectroscopy is used as a stress-sensing technique to analyse the micromechanical response of a range of single carbon fibres in compressive loading. The experimental procedure to produce single fibre compressive stress-strain curves for two high modulus carbon fibres are reported and discussed. An additional technique to utilise Raman spectroscopy to carry out point-to-point, spatially resolved stress mapping a long a length of fibre, from which interfacial shear stress characteristics can be derived is reported. The experimental setup has simpler sample design and preparation methods than other single fibre compression testing techniques, whilst being versatile in the measurements that can be obtained from various carbon fibre types.

1 INTRODUCTION

Characterising the mechanical performance of single carbon fibres under compressive deformation can be a challenge due to the complex and laborious sample preparation and experimental methodologies for many of the commonly used techniques [1]. Laser Raman spectroscopy (LRS) can be utilised to observe and quantify stresses and strains within the atomic structure of graphitic materials such as carbon fibres [2]. Experimental setups for the analysis of single carbon fibres using *in situ* LRS are relatively simplistic when considering sample preparation and deformation methods. Additionally, the technique avoids commonly encountered issues due to fibre aspect ratios such as fibre buckling.

Raman spectroscopy utilises inelastic scattering of monochromatic light to measure atomic bonding information. Vibrational modes in the measured material correspond to bonding types within the atomic structure of the material [3]. The vibrational modes are present in a Raman spectrum as characteristic

bands. Certain vibrational modes within the carbon fibre's spectra experience a shift in their scattering energy when the material is deformed, which corresponds to a shift in the position of the band's position [4]. This shift in the position of the band can be used to derive values of stress and strain within the fibre at any measured point [5]. Point-to-point Raman mapping can be used to analyse stress distributions as well as being used to derive interfacial shear stress along fibre lengths [6]. In this work, LRS is used to characterise single carbon fibres in compressive loading. This enables compressive strain to failure and strength to be determined. Additionally, point-to-point mapping is carried out to analyse the interface of short fibre lengths embedded in a resin composite which is subjected to compressive loading.

2 EXPERIMENTAL

2.1 MATERIALS

Four grades of commercial carbon fibre are used in this study, M46J and M55J high modulus fibres and T300, a standard modulus fibre, supplied by Toray (Toray Advanced Composites, NL). Unsized AS4 HS-CP-5000 carbon fibres used were supplied by Hexcel Composites (Hexcel GB). Reported mechanical properties for each fibre are summarised in Table 1.

Fibre	Tensile Young's Modulus (GPa)	Composite Compressive Strength (MPa)
M46J	436	1090
M55J	540	890
T300	230	1470
AS4	231	1530

Table 1: Datasheet properties for the four carbon fibres investigated. Composite compressive strengths are reported for 60% fibre volume fraction composites with #2500 epoxy for the Toray fibres [7-9].

Poly(methyl methacrylate) (PMMA) used was supplied by Merck (DE). This was supplied in sheet form which was cut into beams. An epoxy resin formulation was used which consisted of a resin, Araldite® LY5052 containing 50-70 % phenol polymer with formaldehyde, glycidyl ether and 30-50% 1,4-Bis(2,3-epoxypropoxy)butane, and a hardener, Aradur® 5052CH, containing 50-70% 2,2'dimethyl-4,4'-methylenebis(cyclohexylamine), 30-50% 3-aminomethyl-3,5,5-trimethylcyclohexylamine, 3-5%, 2,4,6-tris(dimethylaminomethyl)phenol and 1-3% salicylic acid, both provided by Huntsman Corporation (US). A dry film, non-silicone mould release agent, Ambersil Formula 10 was used, provided by RS components Ltd, (GB). C4A-06-015SLA-120-39P strain gauges were supplied by Micro-Measurements group UK Ltd (GB). CN Cyanoacrylate adhesive was supplied by Technimeasure (GB).

2.2 SAMPLE PREPARATION

Four-point bending samples, shown in Fig. 1a, were produced by embedding single carbon fibres into the surface of a PMMA beam. The beam dimensions followed ASTM D6272-17 [10] and were produced by laser cutting, with final dimensions of 64 × 12.5 × 3.13 mm, as seen in Fig. 1b. PMMA was dissolved in acetone, producing a 5 wt% PMMA solution, and used to embed the single fibres into the surface of the PMMA beam, parallel to the length of the beam. Strain gauges were secured to the same face of the beam that the fibres were embedded in, with the gauge's grid parallel to the length of fibre. Cyanoacrylate adhesive was used to adhere the strain gauges to the surface of the PMMA.

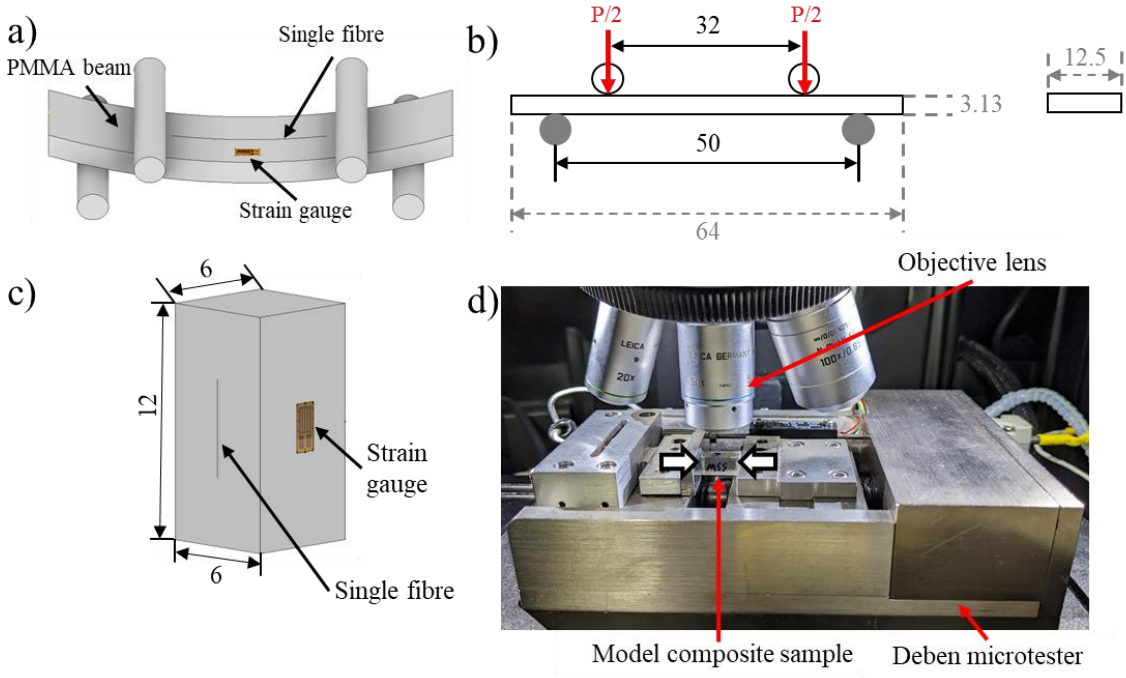

Figure 1: Sample types used in this study. Four-point bending beam a) schematic, b) dimensions and c) epoxy prism model composite schematic and d) a photograph of the uniaxial compression rig in a typical Raman microscope setup. Dimensions are in mm.

Epoxy prism model composites in Fig. 1c used for uniaxial compression of single fibres were produced by mixing a resin (LY5052) and hardener (HY5052) in a ratio of 100:38 parts by weight. The mixture was degassed at full vacuum for 20 min. The epoxy was then cast in a silicone mould coated with release agent. The cast epoxy was left for 7 days to cure at room temperature and pressure to reduce residual stresses from curing. The resulting prisms had dimensions following ASTM D695-15 [11], with final dimensions of 6 × 6 × 12 mm. Short lengths of single fibres (5-7 mm) were then embedded in the surface of the epoxy prisms by adding a thin layer of epoxy onto the cured prism and manipulating the short fibre into the uncured layer and leaving the sample another 7 days to cure. Strain gauges were then adhered to the prisms, with the grid parallel to the length of the fibre. In some cases, two strain gauges were adhered to each side of the sample to ensure no bending was taking place.

2.3 RAMAN ANALYSIS

The Raman spectrometer used was a Renishaw inVia Raman spectrometer with a 532 nm DPSS diode laser, with a maximum power of 200 mW, and a 2400 lines/mm grating. The incident laser light was polarised parallel to the length of the fibre. The microscope used was a Leica DMLM with a long working distance 50× lens to focus the laser to a spot size of 1-2 µm.

Four-point bending was carried out using a custom manual bending rig. The support pins had a separation spacing of 50 mm and the loading pin spacing was 32 mm. Support and loading pins both had circular cross sections with 5 mm diameters. Deformation was applied by a threaded screw rotated to apply force to the loading pins which bent the beam in either tension or compression. Compressive deformation was applied in strain steps of -0.034 %. The laser was initially calibrated against a silicon wafer with a Raman band located at ~520 cm^{-1}. Spectra were obtained by exposing the embedded fibre to the laser at 50% power for 45 seconds. To collect G band peak shift information in four-point bending, measurements were collected from one position at the centre of the fibre, with a Raman wavenumber range of 1200 cm^{-1} to 1750 cm^{-1}. Spectra at each strain step were collected and functions were fitted to the spectra. A fitting method reported by Brubaker et al. was applied to the spectra to obtain the G band

positions [12]. The fitting involved a 4-peak model applied to the D-G region, using pseudo-Voigt functions. The G band positions were then plotted as Raman wavenumber shift versus strain, with the shift in Raman wavenumber of the G band used to calculate stress in the fibre. These stresses were derived using a universal average phonon shift rate of $-5\omega_0^{-1}$ cm^{-1} MPa^{-1}, derived by Frank et al. [13], where ω_0 is the G band position at zero stress. Four-point bending was used to produce a G band shift rate versus strain calibration for each fibre, as well as derive an estimated compressive stress versus strain curve for each fibre.

Single fibres embedded in epoxy prisms were subjected to uniaxial compression using a Deben microtest stage fitted with a 5 kN loadcell. Point-to-point mapping of the position of the G Raman band was used to measure stress along a short length of fibre, which was then converted to interfacial shear stress using Cox's shear lag theory [14]. The Deben stage setup within the Raman microscope enclosure can be seen in Fig. 1d.

Compressive deformation is applied as strain steps, the step size depending on the fibre type. For the standard modulus fibres, a higher compressive strain to failure is expected therefore the applied strain steps are larger. At each level of applied compression, point-to-point mapping is carried out, collecting the position of the G band at each point along the fibre. Strain in the fibre is calculated from the G band shift vs strain calibration at each measured point. Measurement resolution is higher at the ends of the fibre to analyse the transfer length for each sample. At each end of the fibre, or at fibre breaks, measurements are collected every 2 μm until 100 μm, then every 5 μm until 400 μm, then every 50 μm until the middle of the fibre. The same measurement spacing is repeated for the other half of the fibre.

3 RESULTS AND DISCUSSION

The methods employed here are beneficial when compared to other single fibre testing methods, by requiring less laborious sample preparation methods [15], as well as being able to estimate compressive strain to failure and strength.

Typical Raman spectra for all of the fibres are shown Fig. 2a. Due to the microstructural differences between the high and standard modulus fibres, the spectra differ in their resolutions, with the standard modulus fibres having much broader, less well-defined bands when compared to the high modulus filaments. Both sets of fibres have the same Raman bands present in their spectra, with differing intensities and Full Widths at Half Maxima (FWHM). Due to the higher degree of graphitisation in the high modulus fibres, both the G and D bands have smaller FWHMs and band 'sharpening' is observed. The spectral fitting and peak deconvolution is shown in Fig. 2c and 2d. Each peak within the spectra contains vibrational band information which corresponds to bonding and vibrational information within the structure of the carbon fibre. The main band of interest is the G band which has previously been shown to allow stress mapping within graphitic materials [13]. The G band (located at ~1580 $cm^{-1)}$ corresponds to the doubly-degenerate iTO and LO phonons with E_{2g} symmetry at the Brillouin zone centre [15] and is related to the carbon-carbon bond in plane stretching of the graphite planes in an infinite crystal. Due to phonon 'hardening' in compression, the band shifts to higher wavenumbers with the onset of compressive loading [2]. The various D bands are due to vibrational modes within the disordered regions of amorphous carbon in the fibre's microstructure [17].

Four-point-bending with fibres embedded in the compressive face of the PMMA beam was used to obtain G band shift that were characterised for all fibres measured (Fig. 2b.), with shift rates similar to those reported in the literature for the high modulus fibres; M46J and M55J. The shift rates observed under compressive deformation are presented in Table 2.

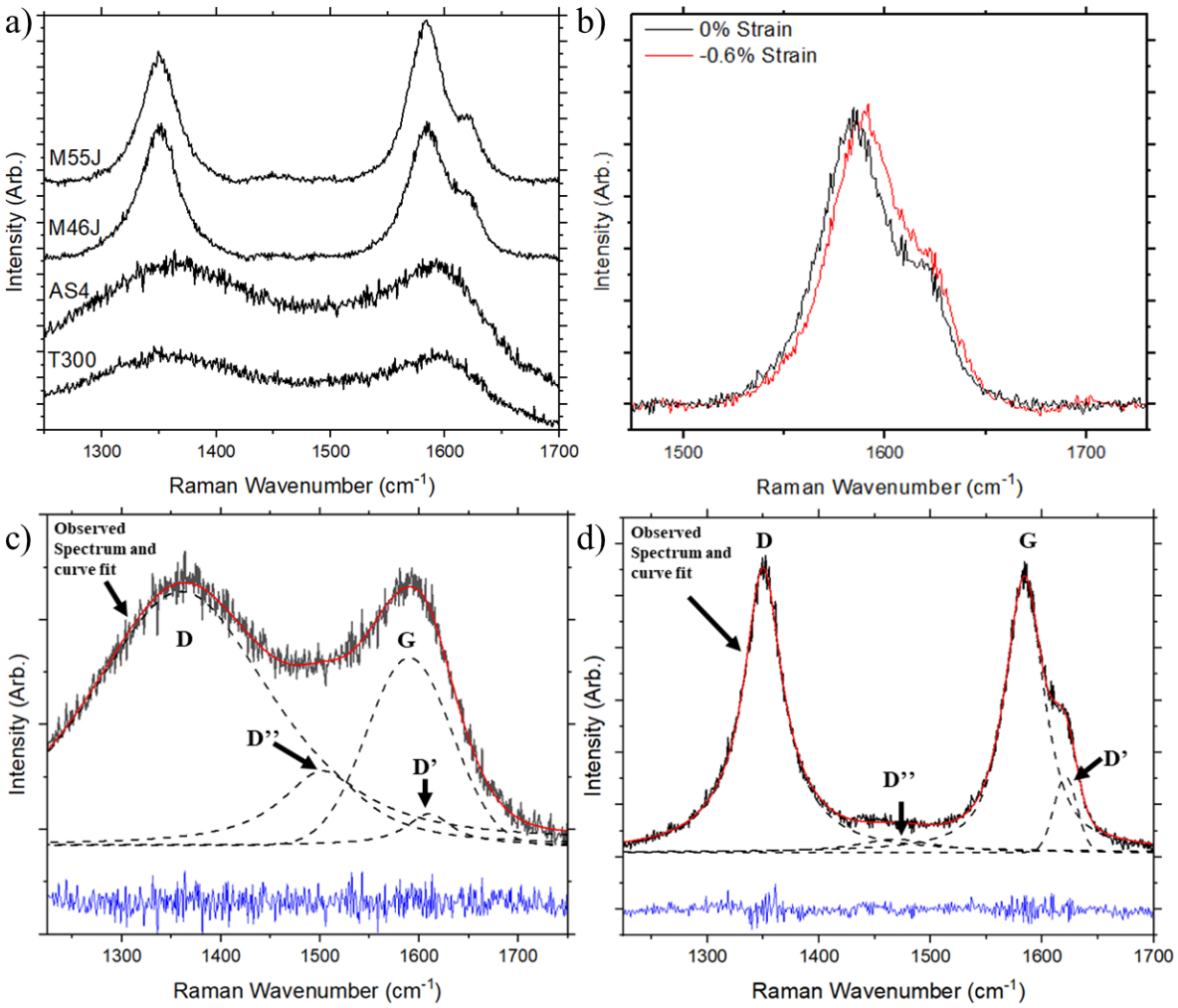

Figure 2: Example Raman spectra for all fibres under investigation, a) demonstrating the difference in spectra between high modulus (M46J, M55J) and standard modulus fibres (AS4, T300), b) the spectral shift for the G band under compressive loading and the spectral deconvolution for c) standard AS4 fibres and d) high modulus M46J fibre's spectra. Blue lines show the residual.

Fibre	Strain Sensitivity (cm^{-1})*	Reported G Band Strain Sensitivity (cm^{-1})*
M46J	9.64 ± 0.2	10.9
M55J	11.68 ± 0.3	11.2
T300	4.70 ± 0.6	N/A
AS4	6.38 ± 0.9	N/A

Table 2: Strain sensitivities of fibre's G band vibrational mode with respect to strain in compression. Reported G band strain sensitivities from [18]. * Strain in percentage.

Using the universal phonon shift rate of $-5\omega_0^{-1}$ cm^{-1} MPa^{-1} for the G band shift, single fibre stress-strain curves have been derived for the two high modulus fibres, shown in Fig. 3 with the derived mechanical properties summarised in table 3.

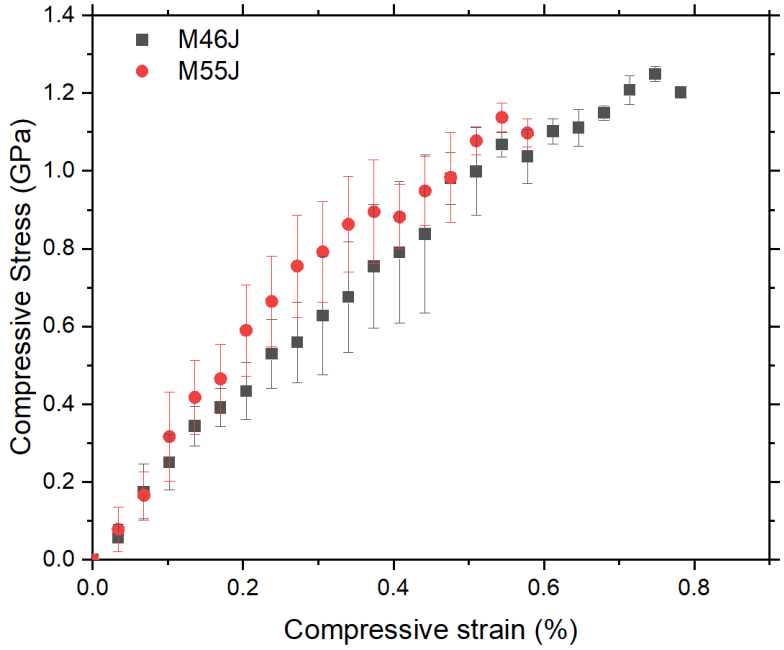

Figure 3: Single fibre compressive stress-strain curves for M46J and M55J high modulus carbon fibres.

Fibre	Compressive Strain to Failure (%)	Compressive Strength (GPa)
M46J	0.64 ± 0.11	1.17 ± 0.07
M55J	0.47 ± 0.10	0.94 ± 0.08

Table 3: Derived mechanical properties for M46J and M55J high modulus carbon fibres.

Single fibre stress-strain data for the two high modulus fibres shows that M46J has a higher strain to failure and compressive strength than the M55J fibres, which is as expected due to the M46J fibres having a lower modulus. Reported single fibre mechanical compression testing via a cantilever setup has been carried out for M55J fibres in which strengths of 1-1.7 GPa were obtained have been discussed in the literature [19, 20]. Here, we report an average compressive strength of 0.94 GPa.

Point-to-point stress mapping has been carried out to produce initial G band position maps for short lengths of high modulus fibres, as described in the experimental methods (Fig. 4). On initial testing it was found that the key sample preparation step is to ensure consistent fibre depth within the sample. The fibre depth must be controlled to be as close to the surface of the epoxy as possible to be able collect spectra with suitably high intensity from the embedded fibres to accurately fit the G band peaks.

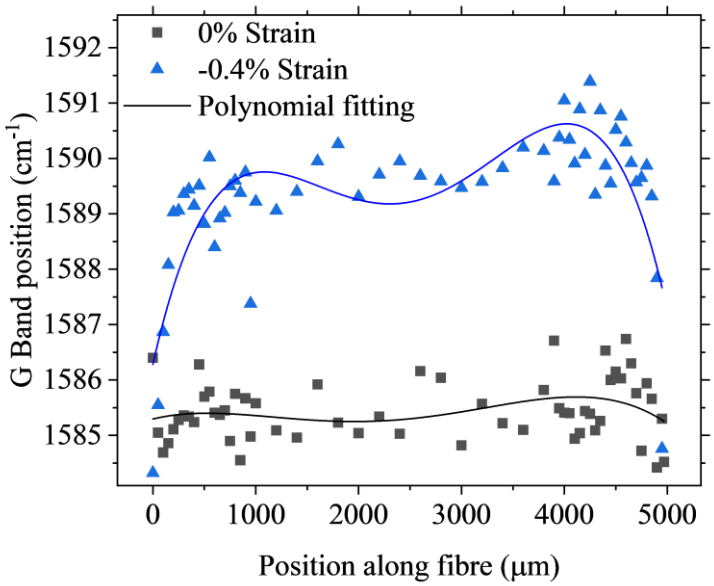

Figure 4: Example point-to-point mapping along a single fibre in a model composite. Demonstrates G band position mapping in compressive loading, with 4th order polynomial fit to demonstrate the shape of the trend in band position.

An example of a stress map is shown in Fig. 4 for an as-received M46J fibre with lower special mapping resolution than intended in the later collections. This demonstration of the technique shows the expected trend in G band is observed with low G band position at the ends of the fibres, which builds quickly to a raised plateau in along the centre of the fibre. The trend shows the G band shift at zero or near zero at the ends of the fibre in compression which is indicative of stress being transferred via shear into the fibre from the matrix [21]. Using this technique, with the stress calibration obtained from four-point bending, the stress along the length of fibre can be derived, along with interfacial shear stress characteristics such as the stress transfer length and maximum interfacial shear stress. Interfacial behaviour such as debonding can be also observed which is typified by a linearisation of the shift in data to constant shear stress, where the interface is then assumed to be entirely frictional [22].

4 CONCLUSIONS AND NEXT STEPS

The methods to measure micromechanical response of single carbon fibres to compression discussed here are under development to obtain both the mechanical properties of single carbon fibres as well as a method to assess the interface of fibres and its effect on compressive performance of model composites in compression. A method for the use of four-point bending to obtain a G band peak shift with respect to strain has been shown and discussed, with single fibre stress-strain behaviour for two high modulus carbon fibres having been derived. Compressive strength and strain to failure are estimated for the fibres from the results achieved using Raman spectroscopy. The use of point-to-point stress mapping as a route to investigate the effect of the fibre-matrix interface on the compressive performance of single fibre model composites has also been discussed.

The next steps in this work will be to produce single fibre compressive stress-strain behaviour for the standard modulus fibres as well as carrying out point-to-point mapping of the model composite single fibres, including with treated interfaces.

ACKNOWLEDGEMENTS

The authors kindly acknowledge the funding for this research provided by UK Engineering and Physical Sciences Research Council (EPSRC) programme Grant EP/T011653/1, Next Generation Fibre-Reinforced Composites: a Full Scale Redesign for Compression a collaboration between University of Bristol and Imperial College London**.**

REFERENCES

[1] S. Nunna, A. R. Ravindran, J. Mroszczok, C. Creighton, and R. J. Varley, A review of the structural factors which control compression in carbon fibres and their composites. *Composite Structures*, **303**, 2023, pp. 116293 (doi: 10.1016/j.compstruct.2022.116293)

[2] Z. Li, L. Deng, I. A. Kinloch and R. J. Young, Raman spectroscopy of carbon materials and their composites: Graphene, nanotubes and fibres. *Progress in Materials Science*, **135**, 2023, pp. 101089 (doi: 10.1016/j.pmatsci.2023.101089)

[3] A. C. Ferrari, and D. M. Basko, Raman spectroscopy as a versatile tool for studying the properties of graphene. *Nature Nanotechnoly*, **8**, 2013, pp. 235–246 (doi: 10.1038/nnano.2013.46)

[4] I. M. Robinson, M. Zakikhani, R. J. Day, R. J. Young and C. Galiotis, Strain dependence of the Raman frequencies for different types of carbon fibres. *Journal of Materials Science Letters*, **6**, 1987, pp.1212–1214 (doi: 10.1007/BF01729187).

[5] N. Melanitis, C. Galiotis, P. L. Tetlow and C. K. L. Davies, Monitoring the micromechanics of reinforcement in carbon fibre/epoxy resin systems. *Journal of Materials Science Letters*, **28**, 1993, pp.1648–1654 (doi: 10.1007/BF00363362).

[6] S. Y. Jin, R. J. Young and S. J. Eichhorn, Controlling and mapping interfacial stress transfer in fragmented hybrid carbon fibre-carbon nanotube composites. *Composites Science and Technology*, **100**, 2014, pp. 121–127 (doi: 10.1016/j.compscitech.2014.05.034).

[7] Toray Composites America Inc, *M46J High Modulus Carbon Fibre*, M46J Rev. 1, 2018. https://www.toraycma.com/wp-content/uploads/M46J-Technical-Data-Sheet-1.pdf

[8] Toray Composites America Inc, *M55J High Modulus Carbon Fibre*, M55J Rev. 2, 2020. https://www.toraycma.com/wp-content/uploads/M55J-Technical-Data-Sheet-1.pdf

[9] Hexcel, *HexTow AS4 Carbon fibre*, CTA 311 JA20, 2020. https://www.hexcel.com/user_area/content_media/raw/AS4_HexTow_DataSheet.pdf

[10] ASTM International, D6272-17, *Standard Test Method for Flexural Properties of Unreinforced and Reinforced Plastics and Electrical Insulating Materials by Four-Point Bending*, 2021 (doi: 10.1520/D6272-17).

[11] ASTM International, D695-15, *Standard Test Method for Compressive Properties of Rigid Plastics*, 2021 (doi: 10.1520/D0695-15)

[12] Z. E. Brubaker, J. J. Langford, R. J. Kapsimalis and J. L. Niedziela, Quantitative analysis of Raman spectral parameters for carbon fibers: practical considerations and connection to mechanical properties. *Journal of Materials Science*, **56**, 2021, pp. 15087–15121 (doi: 10.1007/s10853-021-06225-1).

[13] O. Frank *et al.* Development of a universal stress sensor for graphene and carbon fibres. *Nature Communications*, **2**, 2011, pp. 255–257 (doi: 10.1038/ncomms1247).

[14] M.R. Piggott, *Load-Bearing Fibre Composites*, pp. 83–99, Pergamon Press, Oxford, 1980.

[15] J. Wang, N. Salim, B. Fox and N. Stanford, Anisotropic compressive behaviour of turbostratic graphite in carbon fibre. *Applied Materials Today*, **9**, 2017, pp. 196–203 (doi: 10.1016/j.apmt.2017.07.010).

[16] L. M. Malard, M. A. Pimenta, G. Dresselhaus and M. S. Dresselhaus, Raman spectroscopy in graphene. *Physics Reports*, **473**, 2009, pp. 51–87 (doi: 10.1016/j.physrep.2009.02.003).

[17] A. Sadezky, H. Muckenhuber, H. Grothe, R. Niessner and U. Pöschl, Raman microspectroscopy of soot and related carbonaceous materials: Spectral analysis and structural information. *Carbon*,

N. Y. **43**, 2005, pp. 1731–1742 (doi: 10.1016/j.carbon.2005.02.018).

[18] F. Tanaka, T. Okabe, H. Okuda, I. A. Kinloch and R. J. Young, The effect of nanostructure upon the compressive strength of carbon fibres. *Journal of Materials Science*, **48**, 2013, pp.2104–2110 (doi: 10.1007/s10853-012-6984-z).

[19] C. Wang, B. Zhang and G. Bai, Improved testing method for the compressive strength of single fiber. *Measurement: Journal of the International Measurement Confederation*, **92**, 2016, pp. 193–199 (doi: 10.1016/j.measurement.2016.06.024).

[20] B. Zhang, Y. Wu, Z. Yang and X. Wang, Experimental investigation of the longitudinal compressive strength of carbon fibres with a direct measurement system. *Polymers and Polymer Composites*, **19**, 2011, pp. 477–484 (doi: 10.1177/096739111101900605).

[21] S. Goutianos, T. Peijs and C. Galiotis, Comparative assessment of stress transfer efficiency in tension and compression. *Composites Part A: Applied Science and Manufacturing*, **10**, 2002, pp. 1303–1309 (doi: 10.1016/S1359-835X(02)00166-5).

[22] S. Y. Jin, R. J. Young and S. J. Eichhorn, Hybrid carbon fibre-carbon nanotube composite interfaces, *Composites Science and Technology*, **95**, 2014, pp. 114–120 (doi: 10.1016/j.compscitech.2014.02.015).